Capacitive, inductive and helicon-wave modes of operation of a helicon plasma source

A. R. Ellingboe[a] and R. W. Boswell
Plasma Research Laboratory, Research School of Physical Sciences and Engineering, Australian National University, Canberra, Australian Capital Territory, 0200, Australia

(Received 30 January 1996; accepted 16 April 1996)

Vector-rf-B-field measurements in the near-field of a helicon plasma source taken throughout the volume of the source are reported. Three distinct modes of operation of the helicon plasma source, capacitive, inductive, and helicon-wave, are identified by the structure of the plasma-wave-fields. Results are reported for a double-half-turn antenna, which is believed to be the first reporting for such an antenna structure in application to helicon-wave plasma sources. Comparison is made to a double-saddle-coil antenna which also demonstrates the distinct inductive and helicon-wave modes.
© *1996 American Institute of Physics.* [S1070-664X(96)04807-0]

I. INTRODUCTION

Helicon waves propagate in magnetoplasmas for frequencies (w) between the ion and electron cyclotron frequencies (w_{ci} and w_{ce}) and recently have been found to be very effective in creating high plasma densities both in linear[1–5] and toroidal[6] systems. Typical parameters are: magnetic fields of 5–500 mT, frequencies of 2–40 MHz, and axial wavelengths of 10–50 cm, with such waves producing plasma densities (n_0) of 10^{17}–10^{20} m^{-3}. In non-propagating-wave based inductive discharges, energy penetration is limited to the skin depth resulting in power deposition near the edge of the plasma. Conversely, in a helicon-wave based plasma source, the wave energy can penetrate into the interior of the plasma column resulting in power deposition away from the edges of the source, and therefore the potential for higher peak densities (greater than 10^{19} m^{-3}). High peak densities can be useful for some applications including ion lasers,[5] and plasma based accelerators.[7]

In addition to the ohmic heating from the currents induced by the helicon wave, electrons can become trapped in the traveling helicon wave via the resonance condition given by $\omega - k_{\|} v_{\|} = 0$, where $k_{\|}$ and $v_{\|}$ are the wave vector and electron velocity, respectively, parallel to the axial magnetic field. Typical phase velocities of the helicon wave are such that electrons resonant with the wave have some tens of eV's of energy, where collision cross sections for molecular dissociation and ionization are substantially larger than at thermal energies. By careful antenna/source design, one should be able to control the wave-resonant energy, and thereby control the plasma and gas-phase chemistry. For this to occur, a propagating helicon wave parallel to the axial magnetic field must exist in the plasma and a mechanism must exist to pre-accelerate electrons into the trap-well of the traveling wave. Ellingboe *et al.*[8] have measured significant wave-particle interaction in the near-field of the antenna (less than two wavelengths from the antenna), and have proposed a model for the pre-acceleration scheme.[8,9] In this paper we present select data from an extensive investigation of the wave-fields in the near-field of the antenna to aid in understanding under what experimental conditions trapped electrons can be expected, and how they are accelerated into the wave trap-well. Detailed investigation of this interaction is beyond the scope of this paper and will be discussed in future work.

Considerable emphasis has been placed on the "helicon jump"[10,11] above which the plasma was assumed to be operating with helicon wave heating. A large increase in plasma density (n_0), coupled with decreases in plasma potential (V_p), the Q of the tuning circuit, and the electron temperature (T_e), have been measured across the jump, but direct evidence of a fundamental change in the E-M-mode has not been reported in the literature. Furthermore, some authors have seen multiple jumps,[12,13] which were suggested to be higher order radial eigenmodes, but, again, no detailed confirmation has been reported.

In section IV we present measurements of three-dimensional spatial profiles of the three orthogonal components of the rf B-field in the near-field of a double-half-turn antenna. Based on the rf magnetic wave-fields that exist in the plasma, three distinct modes of operation are identified which we label as capacitive (E-mode), inductive (H-mode) and helicon-wave mode (W-mode). Two dramatic changes in plasma-wave-field profiles ("jumps") are found. The first jump occurs at the E–H mode transition, and the second at the H–W mode transition.

Degeling *et al.*[14] show that in W-mode the measured waves obey the helicon dispersion relation, and that the H–W transition is concurrent with the strong increase in plasma formation in the interior of the plasma column, suggesting that in W-mode, the helicon wave contributes to power deposition and electron heating.

The antenna structure investigated is a double-half-turn antenna (DHT), which contains no current components parallel to the axial magnetic field. We believe this is the first demonstration of the DHT antenna structure in application to helicon wave excitation. For application to surface modification of materials, such an antenna has advantages over Boswell,[1,8] Nagoya-III,[15] and twisted-Nagoya-III[4,16,17] antenna structures in that the length of a double-half-turn sys-

[a]Present address: Lawrence Livermore National Laboratory, Livermore, California 94550.

Downloaded¬19¬Jun¬2008¬to¬150.203.179.67.¬Redistribution¬subject¬to¬AIP¬license¬or¬copyright;¬see¬http://pop.aip.org/pop/copyright.jsp

tem can be considerably shorter. The advantage of short systems has been pointed out in previous work.[18,19]

In section IV D we present some data obtained with a Boswell antenna structure, and show similarities to the DHT antenna structure: In particular, the distinct H-, and W-modes.

II. THEORY

First we follow the method of Cross[20] to derive the linear helicon dispersion relation, investigate the broadcast spectrum of the antenna structure, and then show how the solutions of the dispersion relation can be used to determine the waves in the plasma. Treating the static axial magnetic field as a perturbation to the field-free case, we will discuss magnetic field penetration of the plasma column, resulting in an anomalous skin depth for magnetic field penetration in the direction perpendicular to the axial magnetic field.

A. Helicon dispersion relation

For our experimental conditions (100 G) we satisfy the inequality $\omega_{ci} \ll w \ll \omega_{ce}$, which leads to a simplified ohm's law

$$\vec{E}=\frac{1}{n_e e}\vec{j}\times\vec{B}_0, \tag{1}$$

where $\vec{E}$ is the wave electric field, $\vec{B}_0$ the steady magnetic field, n_e the electron density and $\vec{j}$ the wave current density. We combine Eq. (1) with Maxwell's equations

$$\nabla\times\vec{B}=\mu_0\vec{j} \tag{2}$$

and

$$\nabla\times\vec{E}=-\frac{\partial\vec{B}}{\partial t}, \tag{3}$$

where $\vec{B}$ is the wave magnetic field. For $\vec{B}_0$ in the axial (z) direction and wave field of the form $\exp[i(k\cdot r - wt)]$ where k is the wave vector, one can solve for the natural modes of oscillation for the plasma, yielding[20]

$$k^2\cos(\vartheta)=\frac{\mu_0 n_e e}{B_0}w, \tag{4}$$

where ϑ is the angle between the wave vector $\vec{k}$ and B_0. Taking parallel and perpendicular components of $\vec{k}$ we obtain

$$\sqrt{k_\parallel^2(k_\parallel^2+k_\perp^2)}=\frac{\mu_0 n_e e w}{B_0} \tag{5}$$

from which we can define the dispersion relation

$$D(\omega,k)\equiv\frac{\mu_0 n_e e w}{B_0\sqrt{k_\parallel^2(k_\parallel^2+k_\perp^2)}}-1. \tag{6}$$

The natural modes of oscillation of the plasma are those for which $D=0$. This dispersion relation is for planar geometry; to extend this into cylindrical geometry we use the following definition for $k_\perp$:

$$k_\perp=\frac{\mathscr{Z}(l,n)}{r_{\text{plasma}}}, \tag{7}$$

where $\mathscr{Z}(l,n)$ is the argument giving the nth zero of the lth order Bessel function. An important property of this form of the helicon dispersion relation is that for any combination of plasma parameters there exists a $k_\parallel$ which satisfies $D=0$, and therefore a helicon wave can exist for all densities.

Starting from Eqs. (1)–(3) we can also arrive at[21]

$$\vec{B}=\frac{kB_0}{wn_e e}\vec{j}, \tag{8}$$

which states that the rf currents are ''tied'' to the rf magnetic fields. When there exists rf-B-field from the helicon wave we can expect a corresponding current, resulting in ohmic heating of the bulk, thermal electrons. When there exists B_z, there is j_z driven by E_z, and there can be wave-resonant heating of electrons.

B. Natural modes of antenna–plasma coupling

The $(M,k_\parallel)$ spectrum of the antenna, where M is the azimuthal mode number, can be calculated by taking the Fourier transform of the antenna current:

$$A_{\text{ant}}(M,k_\parallel)=\frac{1}{\sqrt{2\pi}}\int_{-\pi}^{\pi}\int_{-\infty}^{\infty}I_{\text{ant}}e^{ik_z z}e^{iM\theta}dz\,d\theta, \tag{9}$$

where A_{ant} represents the antenna power spectrum and I_{ant} is the antenna current including an image antenna in the conducting plate at $z=0$. For the DHT structure used the spectrum is quite broad, with large amplitudes for wavelengths greater than 1 m, considerably longer than the source tube. The waves present in a cylinder can be represented as a summation:

$$B(r,\theta,z,t)=\sum_{M,k_\parallel}\frac{A_{\text{ant}}(M,k_\parallel)}{D(w,k)}\cos(wt-M\theta-k_\parallel z), \tag{10}$$

where D is the dispersion relation defined in Eq. (6). For an antenna current which varies as $\cos(wt)$, $M\theta+k_\parallel z$ represents the time delay between the antenna current and the local field oscillation at the given (r,θ,z) location. For a plasma with multiple M,k_z modes existing simultaneously,[22] we can define $\Phi_i(r,\theta,z)$ which represents the phase delay between the peak in the field pattern resulting from the interference between the (M,k_z) modes and the peak in the antenna current; the resulting wave amplitude varies as $\cos(wt-\Phi_i)$.

C. Antenna broadcast penetration of the plasma column

The collisionless skin depth can be represented as $\lambda=c/\omega_{pe}$, where $\omega_{pe}=\sqrt{[n_e e^2/(\epsilon_0 m_e)]}$ is the electron plasma frequency, and c is the speed of light. The skin depth represents the plasma's ability to shield out imposed time-varying magnetic fields because of the plasma's conductivity. The skin depth is only valid for $w\ll\omega_{pe}$; for $w\geqslant\omega_{pe}$ the wave is free to propagate as a light wave. At low densities ($n_e\leqslant 10^{15}$ m^{-3}) the skin depth will be less than the source tube diameter. In this case the plasma conductivity is too low to shield out any imposed rf magnetic fields, and the wave-field pattern will be analogous to those which would occur

Downloaded¬19¬Jun¬2008¬to¬150.203.179.67.¬Redistribution¬subject¬to¬AIP¬license¬or¬copyright;¬see¬http://pop.aip.org/pop/copyright.jsp

without the plasma. The plasma will be sustained by the oscillating free charge on the antenna resulting in a capacitive voltage difference between the plasma and antenna. Power is thus transferred to the plasma across the sheath which forms near the antenna. This type of discharge has been investigated extensively and is referred to as an E-type, or capacitive discharge.[23]

As the density increases and the skin depth approaches the chamber diameter, the plasma starts to generate currents throughout its volume to shield out the imposed rf B-field. The induced currents are responsible for power deposition into the plasma. This type of a discharge is referred to as an H-type, or inductive discharge.[23] But the skin depth is actually a measure of the plasma's conductivity: For $w<w_{ce}$ the conductivity in the directions perpendicular to the magnetic field are greatly reduced by the magnetic field. The perpendicular conductivity can be calculated from[24]

$$\sigma_{\text{perp}}=\frac{(\nu_c-iw)w_{ce}}{(\nu_c-iw)^2+\omega_{ce}^2}\sigma_{\text{parallel}}, \tag{11}$$

where ν_c is the electron collision frequency ($\approx 10^7$ s^{-1}) and w_{ce} is the electron cyclotron frequency (1.7×10^9 s^{-1} at 100 G). This results in a considerably larger skin depth for the perpendicular directions. Thus, the B_r and B_θ components can penetrate considerably deeper into the plasma than the B_z component. Recalling Eq. (8), the B_r and B_θ components of the antenna's near-field can couple directly to the helicon wave and the associated currents would ''heat'' the center of the plasma column ohmically. Conversely, the B_z component will be shorted out on the surface of the cylinder, giving power deposition only on the surface. Only if and when the B_z component penetrates into the plasma column do we expect there to be appreciable j_z, increasing ohmic power deposition and allowing the possibility of resonant wave-particle interaction.

III. EXPERIMENT

The experiments are conducted in the large cylindrical plasma apparatus WOMBAT (waves on magnetized beams and turbulence)[25] which consists of two regions, a source and a drift chamber. The source is a Pyrex™ tube 0.18 m inner diameter, 0.5 m long closed by an aluminum plate at one end and opening into a drift chamber 0.9 m diameter, 2 m long at the other end. The system is provided with co-axial solenoidal windings which produce a uniform magnetic field (B_0), parallel to the machine's axis (z), of 10 mT throughout the source decreasing monotonically from the end of the source to 3.5 mT at 0.5 m into the drift chamber ($z=1$ m). The sense of the current in the electromagnet coils is such that $\vec{B}$ is in the $-\hat{z}$ direction. The antenna is a double-half-turn coil (Fig. 1) with the 13.56 MHz rf (radio frequency) power feed at the top, and the antenna terminated into a ground shield which surrounds the source at $r=180$ mm and is connected to the match-box ground.

The system operates with 20 sccm argon continuously flowing through the system resulting in a neutral pressure of 0.25 Pa, and up to 2.5 kW rf power applied to the antenna matching circuit. Typical plasma parameters are, $n_e\approx 3\times 10^{17}$ m^{-3}, $T_e\approx 3$ eV, and plasma potential of ≈ 15 V.

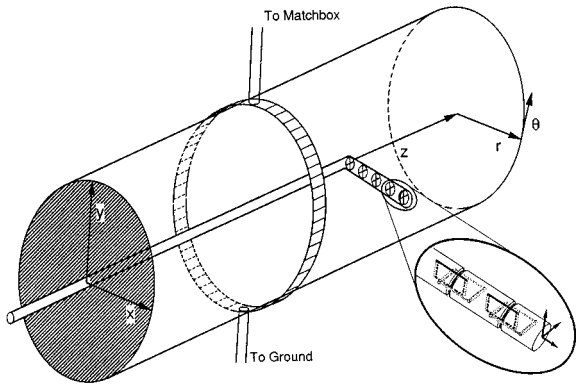

FIG. 1. Schematic of WOMBAT source region. Shown are the double-half-turn antenna, the ground-shield, and the five radii vector-B-dot probe.

A. Diagnostics

Diagnostics include a 10 GHz microwave interferometer measuring the line-integrated plasma electron density across the cord at $z=45$ cm, $\theta=-10°$, where θ is the azimuthal angle (Fig. 1); a Langmuir probe positioned at $z=1.12$ m, $r=0$ cm biased to -80 V to measure ion saturation current; forward and reflected rf power measurements, and antenna voltage and current measurements. To measure the plasma-wave-fields, a five-radial-position ($r_0=$ 0, 2, 4, 6, 8 cm) vector ($\hat{r},\hat{\theta},\hat{z}$ directions) magnetic probe is inserted into the source (Fig. 1). The actual ($\hat{r},\hat{\theta},\hat{z}$) coils are at r_0+3 mm, r_0+2 mm, and r_0+4 mm, respectively. The probe consists of an L-shaped re-entrant Pyrex tube (Fig. 1). The long side of the L is parallel to the axis, at $r=0$ cm. The short side of the L points radially coming within 0.2 cm of the source tube which defines the radial edge of the plasma. A boron-nitride form is inserted into the radial section of the re-entrant tube. At each of the 5 radial positions, three 5-turn inductors are wound on the form and oriented to measure the $\hat{r}$, $\hat{\theta}$, and $\hat{z}$ directions of the magnetic field at that point (Fig. 1, detail). The probe can be manipulated to allow measurement across the radius for any azimuthal (θ) position, and axial position in the range 3 cm$\leqslant z\leqslant$50 cm. The signal from each inductive-loop is carried out along the length of the re-entrant tube as a twisted-pair. Once outside the plasma chamber, the twisted pair signal is fed into a hybrid combiner[26] to remove unwanted capacitive pickup. All rf signals (B-dot-probe and antenna measurements) are fed into a multi-channel quadrature interferometer from which the signal amplitude and phase with respect to the antenna current is obtained. Output from all diagnostics are simultaneously digitized with 12 bit digitizers.

B. Experimental procedure

Two sets of experiments are performed. The first experiment consists of positioning the vector-B-dot probe at a fixed θ and z position. Data are collected as the power is ramped

Downloaded¬19¬Jun¬2008¬to¬150.203.179.67.¬Redistribution¬subject¬to¬AIP¬license¬or¬copyright;¬see¬http://pop.aip.org/pop/copyright.jsp

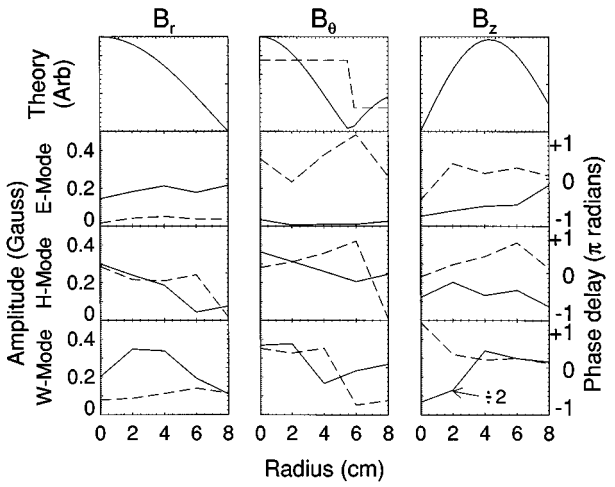

FIG. 2. Radial plots of wave-fields from theory and measured at $z=45$ cm, $\theta=0°$, for E-mode (0.5 kW), H-mode (1.1 kW), and W-mode (1.6 kW) plasmas.

from 0 to 2.3 kW over a 4 s period. The digitizer is clocked at 200 samples/s, yielding 800 data points per shot, or 1 data point for every 3 W increase in forward power. The second set of experiments is conducted by fixing the rf power and the B-dot probe axial position. The probe is rotated 360° in azimuth during a 5 s plasma pulse. The probe's θ position is measured using a potentiometer in conjunction with a voltage source, and this signal is simultaneously digitized with the signals from all system diagnostics. In this way an $r-\theta$ slice of the plasma-wave-fields is obtained.

IV. EXPERIMENTAL RESULTS

A. Introduction

The measured radial profiles of the rf wave-fields at a fixed azimuth ($\theta=0°$) and axial position ($z=45$ cm), for three powers which we will identify as being in E-mode (0.5 kW), H-mode (1.1 kW), and W-mode (1.6 kW) are shown in Fig. 2.

The top row of graphs in Fig. 2 shows the expected theoretical radial profiles for the lowest radial mode. Along with the B_θ component is plotted the expected Φ_{B_θ}: Note the π phase change at the minimum in B_θ amplitude.

The second row of graphs in Fig. 2 show the wave-fields in E-mode, and are analogous to the vacuum fields of the antenna. The B_r component is large and uniform, and results from the $I_{y,\mathrm{ant}}$ (see Fig. 1 for definitions of $\hat{x}$ and $\hat{y}$ orientations) component in each segment of the antenna. The B_r (magnetic fields) induced by $I_{y,\mathrm{ant}}$ interfere constructively. Likewise, B_θ results from the I_x components of the antenna whose induced fields (B_r) interfere destructively on the $y=0$ plane. B_z is dominated by the I_θ currents of the half-turn antenna segments and such fields interfere destructively. With increasing radius, the disparity in distance from the two half-turn coils increases, thus the resultant B_z signal increases. The radial current feed sections of the antenna interfere destructively with the net signal from the I_θ segments, but the I_θ currents dominate for this probe position.

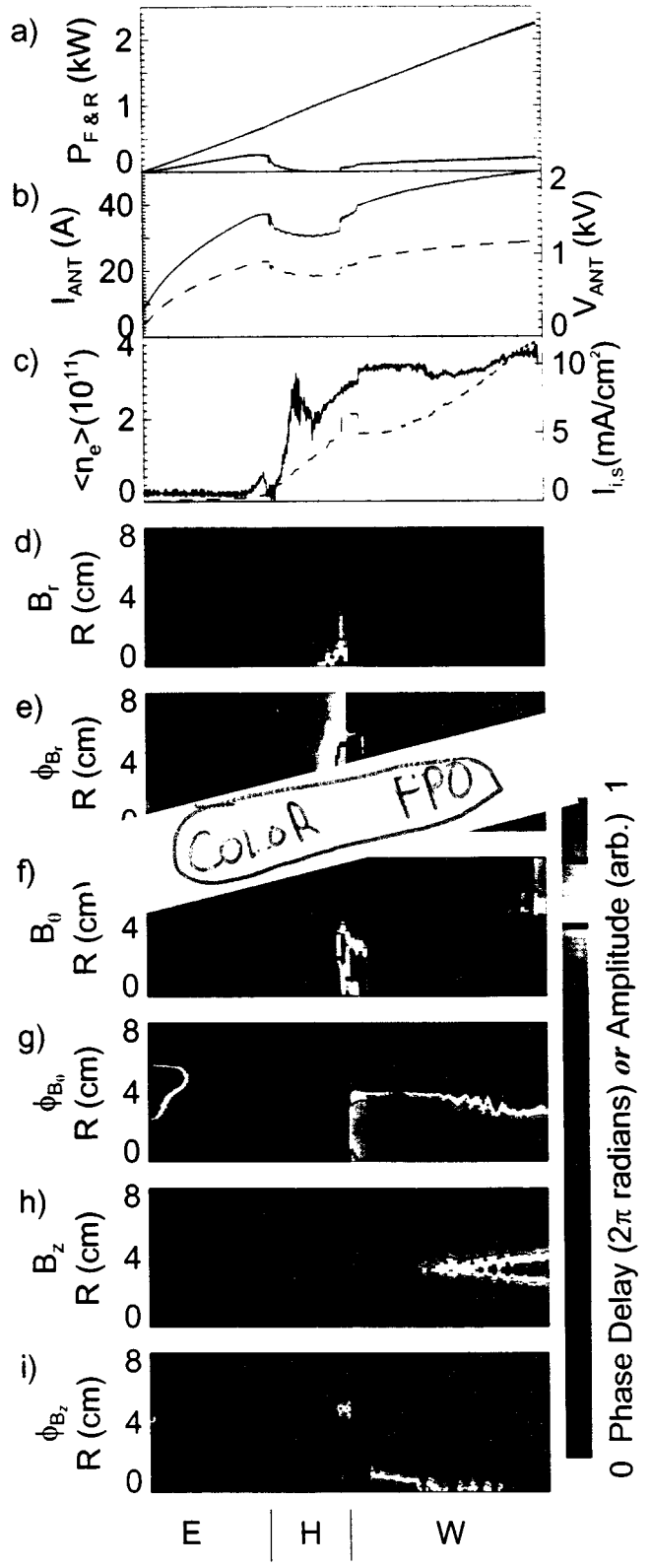

FIG. 3. Measured values vs time (arbitrary) (a) forward and reflected power, (b) antenna current (solid) and voltage (dashed), (c) line-averaged density at $z=45$ cm, $\theta=-10°$ (solid), and ion saturation current at $z=1$ m, $r=0$ cm (dashed). (d–i) radial profiles of components of $\dot{B}$ and phase delay with respect to the antenna current.

The third row of graphs shows the wave-fields in H-mode. In H-mode, B_z is largely excluded from the plasma (this will be more evident in Figs. 3 and 4), and B_r and B_θ

Downloaded¬19¬Jun¬2008¬to¬150.203.179.67.¬Redistribution¬subject¬to¬AIP¬license¬or¬copyright;¬see¬http://pop.aip.org/pop/copyright.jsp

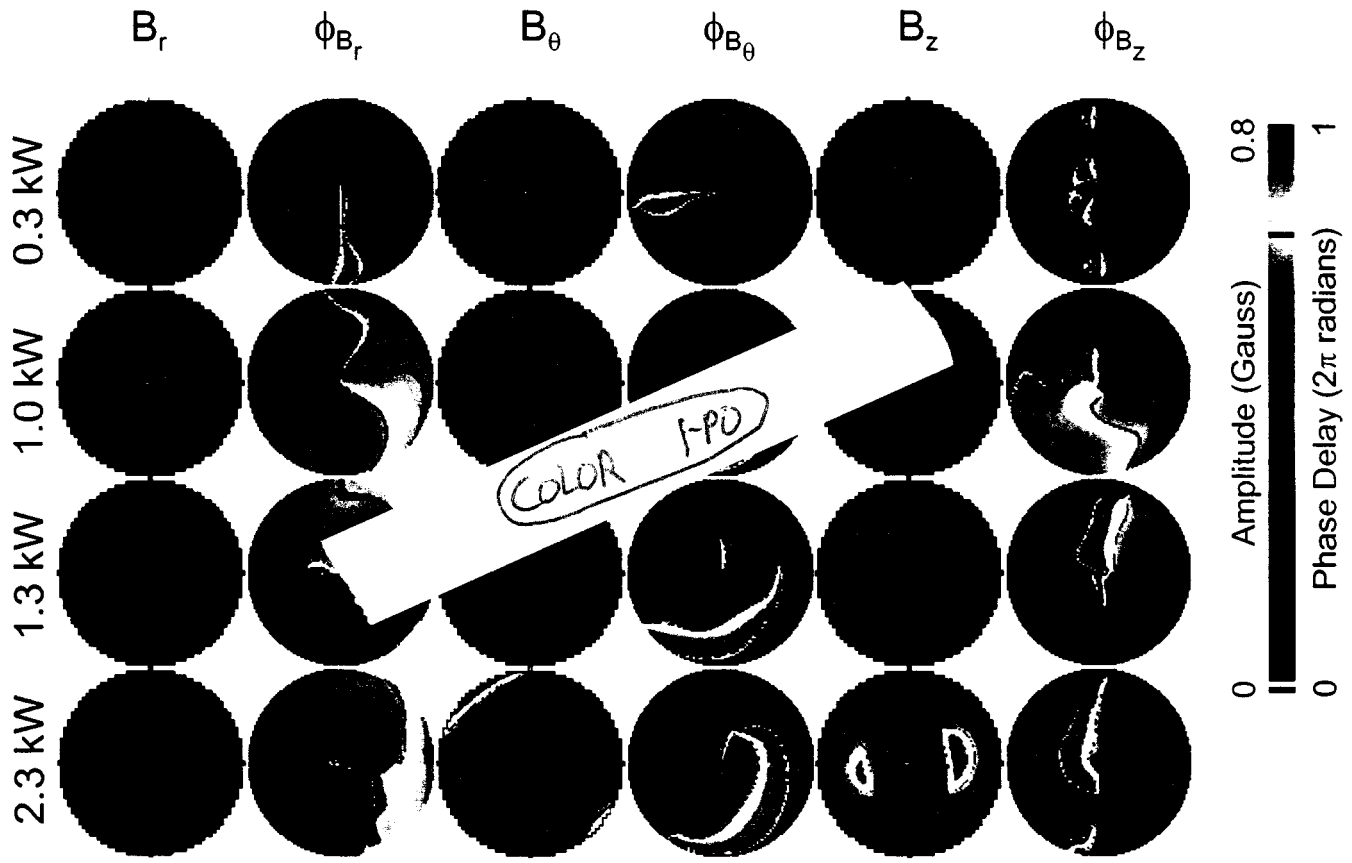

FIG. 4. $\langle r\ -\ \theta \rangle$ color contours at $z=45$ cm plots of plasma-wave-fields at four different powers. The four powers, 0.3, 1.1, 1.3, and 2.0 kW, correspond to E-, H-, W-, and W-mode regions of operation.

both peak at $r=0$ as expected for a traveling wave. However, the phase delay for B_θ varies slowly with radius, and does not exhibit the expected π phase change interior to the plasma.

The bottom row of graphs in Fig. 2 shows the wave-fields in W-mode. Here B_z now exhibits the expected J_1 Bessel function radial dependence. Note that the B_z amplitude is approximately twice that of the B_r and B_θ components. The Φ_{B_θ} now exhibits a π change between $r=4$ cm and $r=6$ cm. The B_r profile is *not* as expected for a pure $M=+1$ wave, and will be discussed when we investigate the azimuthal mode structure which exists in W-mode (Fig. 4).

B. Measured parameters during a power ramp

Figure 3 shows data for a power scan with the probe positioned at $z=45$ cm and $\theta=0°$. Along the ordinate are labeled the E, H, and W-mode regions, along with approximate boundaries for the modes. Figures 3(a–c) show the rf power, antenna current and voltage, and plasma density measurements, respectively. Figs. 3(d,f,h) show two-dimensional color contours of wave-field amplitudes (A_i), and Figs. 3(e,g,i) show their respective phase-delays (Φ_i).

In E-mode, the antenna current and voltage increase approximately as the square root of the power (Fig. 3b), as would be expected for an antenna under constant load. The B_z amplitude increases with the antenna current, and peaks

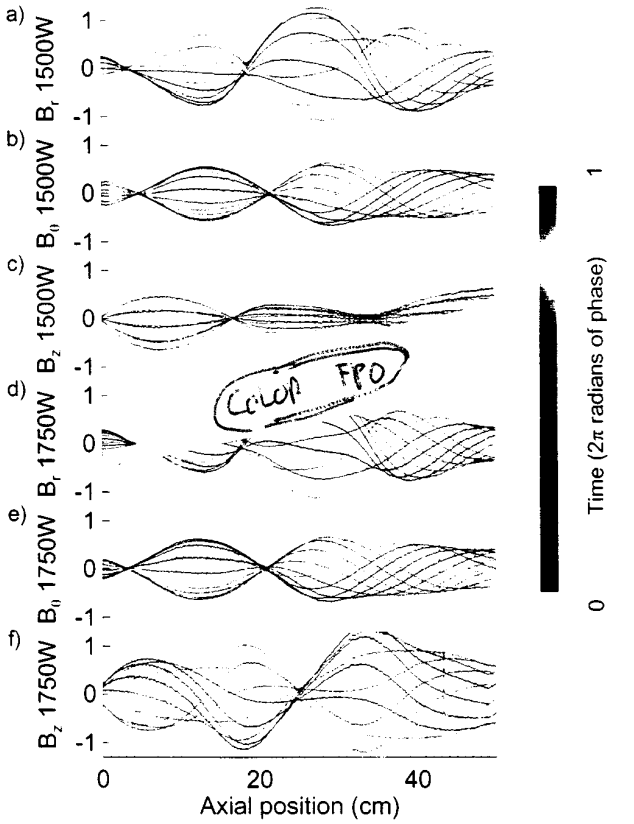

FIG. 5. Plasma-wave-fields for a double-saddle-coil antenna structure. Data are taken vs z, at $r=4$ cm, $\theta=0°$. Data are plotted for a variety of times within the rf cycle.

Downloaded¬19¬Jun¬2008¬to¬150.203.179.67.¬Redistribution¬subject¬to¬AIP¬license¬or¬copyright;¬see¬http://pop.aip.org/pop/copyright.jsp

near the edge due to geometric effects as described in section IV A; B_r is approximately constant in r and increases with the antenna current, and B_θ remains approximately zero. The ion saturation current, and thus plasma density, increases very slowly with increasing power.

As we transfer into H-mode, the reflected power drops, as do the antenna voltage and current; the plasma now loads the antenna strongly. The density increases dramatically, both as measured with the Langmuir probe and the microwave interferometer. (The apparent drop in line-averaged electron density in the initial H-mode phase is due to reflections of the 10 GHz probe-beam off the ground-shield, producing standing-wave interference. This has been confirmed using a 35 GHz interferometer.) In this regime, the edge dominant B_z component is quickly excluded from the plasma. The B_r and B_θ components peak at $r=0$ cm, and have uniform phase across the radius. There is an approximately $\pi/2$ phase difference between B_r and B_θ at $r=0$ mm, identifying the wave as dominantly $M=+1$.

With the transition into W-mode, both the antenna current and antenna voltage increase, which is indicative of a decrease in radiation resistance (plasma loading). Coupled with the increase in reflected power (Fig. 3a), the net power into the plasma decreases. However, the density diagnostics actually show a modest increase in plasma density, suggesting that the W-mode power coupling mechanism is more efficient. From Fig. 3(h) it is evident that above the H–W transition the B_z wave-field again penetrates into the interior of the plasma column. As we move further above the transition (i.e., power is increased) B_z at $r=4$ cm increases, while B_z at $r=8$ cm remains constant. The B_θ component displays a minimum near $r=4$ cm, with the position of the minimum decreasing with increasing power. The corresponding phase component (Φ_{B_θ}) exhibits a π phase change between $r=4$ cm and $r=6$ cm, where the amplitude is a minimum, which agrees with the expected J_0 Bessel function radial profile.

C. Azimuthal structure of plasma wave-fields

Figure 4 contains $(r-\theta)$ maps of the plasma-wave-fields at $z=45$ cm for power levels of 0.3, 1.0, 1.3, and 2.3 kW, which are in the E-, H-, W-, and W-mode regions, respectively. As before, the absolute amplitude and relative-phase-delay are plotted. One can calculate the instantaneous wave-fields from

$$B_i(r,\theta,t)=A_i(r,\theta)\cos[wt-\Phi_{B_i}(r,\theta)], \tag{12}$$

where i denotes the component of the wave-field r,θ, or z. At 0.3 kW the dominant fields are in the $\hat{x}$ direction as can be seen in the B_r and B_θ components (as the probe is rotated through θ, the alignment of $\hat{r}$ or $\hat{\theta}$ with respect to $\hat{x}$ changes). There is a π phase change in Φ_{B_r} at $x=0$ due to $+\hat{r}$ coordinate definitions. Likewise, for Φ_{B_θ} there is a π phase change at $y=0$. The B_z data show the increase in field with increasing absolute value of x, and the Φ_{B_z} data show a π phase change at $x=0$, showing that the two $I_{\theta\,\mathrm{ant}}$ currents impose B_z in opposite sense ($+I_\theta$ gives B_z and $-I_\theta$ gives $+B_z$).

At 1.0 kW (H-mode), the B_z component is small, fairly uniform, and slightly edge-dominant (note the peaks at $\theta=45°$ and 225°). The Φ_{B_z} exhibits a complicated structure which is not understood. The B_r and B_θ components are not uniform in θ; in fact, at 90° rotation off their respective maxima are minima which are very nearly zero. This is a standing-wave in θ. Upon close examination of the phase information (Φ_{B_r} and Φ_{B_θ}) it is evident that where the amplitude is large the phase is nearly constant, and where the amplitude goes through a minimum the phase changes quite rapidly.

The combination of B_r and B_θ yield a plane polarized wave, with orientation of $\theta=30°$. If there is a mix of azimuthal modes (different M values), of nearly equal amplitude the different modes will beat against each other, forming a partially or completely standing wave (the antenna structure has equal-amplitude components for $M=+1$ and $M=-1$, so this standing wave is not too surprising). Looking at Φ_{B_r} and Φ_{B_θ}, they have peaks oriented 90° with respect to each other. However, moving radially from center to edge at $\theta=120°$ or 300° (along the peak in the B_θ signal), Φ_{B_θ} does not exhibit the expected π phase change.

At 1.3 kW (early in W-mode), the B_r component still exhibits the standing wave pattern in θ, but the orientation is rotated (from the H-mode case) by $\approx 50°$. The interior pattern in the B_θ signal also exhibits the standing wave pattern in θ, and the orientation is also rotated by $\approx 50°$. The Φ_{B_θ} now exhibits a π phase change between $r=4$ cm and 6 cm at $\theta=0°$ and 180° (aligned with the peaks in the interior B_θ signal). At $\theta=120°$ and 300° there are large amplitude B_θ components on the edge of the plasma column. These are caused by the near-field (inductive skin depth) penetration of fields from the radial components of the double-half-turn antenna structure, and this has been confirmed experimentally.

Further increases in power (see Fig. 4, 2.3 kW data) give rise to modest amplitude increases of B_r and B_θ-edge fields, and substantial increases in the B_z peak at $r=4$ cm. The amplitude of the $B_z(r=4\text{ cm})$ is roughly proportional to I_{ant} above an apparent threshold of 25 A: $[B_z(r=4\text{ cm}) \propto I_{\mathrm{ant}}-25]$. The exact meaning of this threshold is unclear.

D. Boswell antenna results

Finally, wave-field data utilizing a double-saddle-coil (Boswell)[1,8] antenna are presented. The experimental setup is very similar to the DHT conditions presented above. This antenna extends from $z=18$ cm to 32 cm, with the power feed at $z=18$ cm end.[8] In Fig. 5, instantaneous wave-field amplitudes vs z and t (time represented by different colors) are presented for data from $r=4$ cm, $\theta=0°$. Figures 5(a–c) are the B_r, B_θ, and B_z at 1.5 kW (H-mode in this case), and Figs. 5(d–f) are the B_r, B_θ, and B_z at 1.7 kW (W-mode). The only significant difference between the H- and W-mode wave-fields is in the B_z component. In H-mode, the B_z component is a standing-wave everywhere. In W-mode, B_z is made up of large amplitude standing waves under the antenna θ currents. Downstream (to the right) the wave becomes a traveling wave, and upstream it becomes a partially standing, partially traveling wave. The B_r and B_θ data are

Downloaded¬19¬Jun¬2008¬to¬150.203.179.67.¬Redistribution¬subject¬to¬AIP¬license¬or¬copyright;¬see¬http://pop.aip.org/pop/copyright.jsp

very similar below vs above the transition. Both show standing wave patterns to the left (caused by reflections off of the grounded end plate) and traveling waves to the right of the antenna. The B_r envelope does *not* have the same amplitude as the B_θ envelope, suggesting elliptically polarized waves, or perhaps even plane polarized, as is the case for the double-half-turn antenna structure presented earlier. The polarization of the wave is $M=+1$, both in E- and H-modes, and both in the traveling wave regions and the standing wave regions.

V. DISCUSSION

The existence of the distinct H-mode region poses certain problems in understanding the antenna coupling mechanism. The B_r and B_θ wave-field components obey the helicon dispersion relation in the H-mode region, with their axial wavelength decreasing with increasing density. Upon crossing into W-mode, their axial wavelengths *increase*, then decrease with further increases in density. The axial wavelength variations are consistent with a change in $k_\perp$ from [see Eq. (7)] $\mathscr{Z}(1,0)$ to $\mathscr{Z}(1,1)$ occurring at the H- to W-mode transition, causing the B_z component to be cut-off below the transition. In Figs. 3 and 4, the B_r and B_θ radial profiles show a dramatic reduction in radial extent, in support of the change in $k_\perp$. In H-mode, B_r and B_θ can couple directly into the cylinder (II C) and then propagate axially as a purely electromagnetic helicon wave (no electrostatic component therefore $E_z=B_z=0$). This is equivalent to the solution to the cylindrical wave-guide mode in a conducting shell with infinite parallel conductivity.[21] We have successfully modeled the E- and W-modes of operation using the ANTENA[27] code where we observe the ''turn-on'' of the first radial eigenmode (E- to W-mode transition) at the densities where the experiment transfers into W-mode. However, the H-mode region is not seen, nor is the W-mode turn-on as abrupt as in the experiment. Details of this modeling work are beyond the scope of this paper, and will be discussed in detail in future work. The H- to W-mode transition could be the result of sufficient wave-particle interaction increasing the axial resistivity, to increase penetration of the B_z and E_z. The scenario—interaction increasing penetration increasing interaction—provides positive feedback, and is consistent with the apparent change in mode.

One question which has puzzled the authors is which elements of the antenna structures are important/dominant in coupling power to the helicon wave. The DHT antenna structure is identical to a single end of a Nagoya type III (III) or twisted-Nagoya type III (t-III) antenna. Light and Chen[28] has proposed a physical picture for how the III and t-III antennas couple into the plasma column based on plasma currents which are ''images'' of the *axially aligned* antenna currents, those with a component of their current parallel to the magnetic field. Considering only the axially aligned currents, both III and t-III antenna structures are *half*-wavelength structures: Both have a maximum in their broadcast spectrums at wavelengths twice the length of the antenna. In contrast, considering only the DHT-like end currents the III antenna is a half-wavelength structure, and the t-III is a *full* wavelength structure. Ellingboe and Boswell[29] have operated their helicon source with two-double-half-turn antennas to ''mimic'' the end currents of the III and t-III antenna structures. They powered the antennas both anti-phase and in-phase to mimic the III and t-III end currents, respectively. In W-mode the two antenna structures were found to couple waves into the plasma as half-wavelength and full-wavelength structures as expected, and, for a constant magnetic field, the resultant plasma densities differing by approximately a factor of two, as expected from the helicon dispersion relation, Eq. (6). This suggests that the end-currents can directly couple to the B_z component of the helicon wave, and contribute to antenna-wave coupling. This brings into question modeling work which ignores currents perpendicular to the axial magnetic field.[28,30] However, recent results[30] using a t-III antenna found plasma wavelengths approximately twice the antenna length, suggesting the axially aligned currents were dominant.

VI. CONCLUSIONS

We have presented data which show that the helicon plasma source can operate in three distinct modes. The three modes have been identified as E-mode, in which the plasma has negligible impact on the structure of the magnetic field imposed by the antenna; H-mode, in which the B_z component of the imposed antenna fields is excluded from the bulk of the plasma; and W-mode, in which the B_z plasma wave fields agree with theory for helicon waves. Only in W-mode, where there are $\hat{z}$ components to the magnetic field, do we expect there to be any resonant electron-wave interaction.

The existence of the H-mode, in which the propagating B_z wave-fields do not exist, has broad implications for identification of the helicon-wave mode, as many of the H-mode plasma parameters (matching circuit Q, bulk T_e, peak n_i, V_p, ...) agree with what is expected for W-mode. Researchers may incorrectly identify a H-mode plasma as W-mode. Thus, using only a subset of the plasma parameters for mode identification not including the plasma-wave-fields may not give true identification of the electromagnetic mode of the plasma: The potential for W-mode to produce non-thermal components in the electron-energy-distribution-function (pulsed beams or high energy tails) through resonant electron-wave interaction could cause plasma density profiles and gas-phase chemistry of reactive plasmas to be very different between H-mode and W-mode plasmas.

ACKNOWLEDGMENTS

The authors are grateful for the technical assistance of P. Alexander, J. Anderson, and S. Hyde. The first author is grateful to the staff of the Plasma Research Laboratory at the Australian National University for many stimulating and helpful discussions.

[1] R. W. Boswell, Ph.D. thesis, Flinders University of South Australia, 1970.
[2] R. W. Boswell, Plasma Phys. Controlled Fusion **26**, 1147 (1984).
[3] F. F. Chen and G. Chevalier, J. Vac. Sci. Technol. A **10**, 1389 (1992).
[4] A. Komori, T. Shoji, K. Miyamoto, J. Kawai, and Y. Kawai, Phys. Fluids B **3**, 893 (1991).
[5] P. Zhu and R. W. Boswell, Phys. Rev. Lett. **63**, 2805 (1989).
[6] P. K. Loewenhardt, B. D. Blackwell, R. W. Boswell, G. D. Conway, and S. M. Hamberger, Phys. Rev. Lett. **67**, 2792 (1991).
[7] F. F. Chen, Laser Part. Beams **7**, 551 (1989).

Downloaded¬19¬Jun¬2008¬to¬150.203.179.67.¬Redistribution¬subject¬to¬AIP¬license¬or¬copyright;¬see¬http://pop.aip.org/pop/copyright.jsp

[8]A. R. Ellingboe, R. W. Boswell, J. P. Booth, and N. Sadeghi, Phys. Plasmas **2**, 1807 (1995).
[9]A. R. Ellingboe and R. W. Boswell, Bull. Am. Phys. Soc. **39**, 1460 (1994).
[10]R. W. Boswell, A. J. Perry, and M. Emami, J. Vac. Sci. Technol. A **7**, 3345 (1989).
[11]A. J. Perry, D. Vender, and R. W. Boswell, J. Vac. Sci. Technol. B **9**, 310 (1991).
[12]R. W. Boswell and R. K. Porteous, Appl. Phys. Lett. **50**, 1130 (1987).
[13]A. W. Molvik, T. D. Rognlien, J. A. Byers, R. H. Cohen, A. R. Ellingboe, E. B. Hooper, H. S. McLean, B. W. Stallard, and P. A. Vitello, ''Experiments and modeling of a helicon plasma source,'' to appear in J. Vac. Sci. Technol.
[14]A. W. Degeling, C. O. Jung, R. W. Boswell, and A. R. Ellingboe, Phys. Plasmas **3**, 2788 (1996).
[15]T. Watari, T. Hatori, R. Kumazawa, S. Hidekuma, T. Aoki, T. Kawamoto, M. Inutake, S. Hiroi, A. Nishizawa, and K. Adati, Phys. Fluids **21**, 2076 (1978).
[16]F. F. Chen, in *High Density Plasma Sources*, edited by O. A. Popov (Noyes, Park Ridge, NJ, 1994).
[17]M. Light and F. F. Chen, Phys. Plasmas **2**, 4 (1995).
[18]N. Jiwari, T. Fukasawa, H. Kawakami, H. Shindo, and Y. Horiike, J. Vac. Sci. Technol. A **12**, 4454 (1994).
[19]J. E. Stevens, M. J. Sowa, and J. L. Cecchi, J. Vac. Sci. Technol. A **13**, 2476 (1995).
[20]R. Cross (private communication).
[21]F. F. Chen, Plasma Phys. Controlled Fusion **33**, 339 (1991).
[22]R. T. S. Chen, R. A. Breus, S. Gross, N. Hershkowitz, M.-K. J. Hsieh, and J. Jacobs, Plasma Sources Sci. Technol. **4**, 337 (1995).
[23]H. U. Eckert, *Proceedings of the Second Annual International Conference on Plasma Chemistry and Technology*, edited by H. Boenig (Technomic, Lancaster, PA, 1986), and references within.
[24]J. A. Bittencourt, *Fundamentals of Plasma Physics* (Pergamon, New York, 1986). Equation 5.4: Frequency dependent Hall conductivity. Helicon waves are dominated by Hall currents, as evident from the definition for Ohms law [Eq. (1)] used in this paper.
[25]R. W. Boswell and P. J. Kellog, J. Geophys. Res. Lett. **10**, 565 (1983).
[26]G. G. Borg and R. C. Cross, Plasma Phys. Controlled Fusion **29**, 681 (1987).
[27]See National Information Service Document No. DE85004960 (B. McVey, Plasma Fusion Center, Massachusetts Institute of Technology, Report No. PFC/RR-84-12). Copies may be ordered from the National Technical Information Service, Springfield, VA 22161.
[28]M. Light and F. F. Chen, Phys. Plasmas **2**, 1084 (1995).
[29]A. R. Ellingboe and R. W. Boswell, Bull. Am. Phys. Soc. **39**, 1460 (1994).
[30]M. Light, I. D. Sudit, F. F. Chen, and D. Arnush, Phys. Plasmas **2**, 4094 (1995).

Downloaded¬19¬Jun¬2008¬to¬150.203.179.67.¬Redistribution¬subject¬to¬AIP¬license¬or¬copyright;¬see¬http://pop.aip.org/pop/copyright.jsp